Memo version 4.8.1

BESIII Analysis Memo

BAM-531

July 12, 2022

First measurement of $\psi(3686) \to \Sigma^-\bar{\Sigma}^+$ at BESIII

Yunlong Xiao*[a], Liang Liu[b], and Liang Yan†[1a]

[a]*Fudan University, People's Republic of China*
[b]*University of Science and Technology of China, People's Republic of China*

Internal Referee Committee

Alaa Dbeyssi (Chair)[1], Jifeng Hu[2], and Cui Li[3]

[1]*Helmholtz Institute Mainz, Mainz, Germany*
[2]*South China Normal University, People's Republic of China*
[3]*Qufu Normal University, People's Republic of China*

DocDB : https://docbes3.ihep.ac.cn/cgi-bin/DocDB/ShowDocument?docid=1014

Hypernews : http://hnbes3.ihep.ac.cn/HyperNews/get/paper531.html

Abstract

Using data of $(448.1 \pm 2.9) \times 10^6$ $\psi(3686)$ taken with the Beijing Spectrometer (BESIII) at the Beijing Electron-Positron Collider(BEPCII) in 2009 and 2012 year, the process $\psi(3686) \to \Sigma^-\bar{\Sigma}^+$ has been measured exclusively. The branching fraction of $\psi(3686) \to \Sigma^-\bar{\Sigma}^+$ is measured to be $(2.83 \pm 0.04 \pm 0.08) \times 10^{-4}$ for the first time. The parameter value of $\alpha_{\psi(3686)}$ is measured to be $0.96 \pm 0.09 \pm 0.03$ for the first time.

*xiaoyl20@fudan.edu.cn
†yanl@fudan.edu.cn

Contents

1 Introduction

The angular V distribution of the baryon states is a very interesting topic. Actually, V is instead of a charmonium vector like $J/\psi, \psi(3686)$. In the limit of infinitely heavy charm mass, the hadron helicity conservation rule implies α= 1 [1]. The values of angular distribution of $J/\psi \to \Sigma^+\bar{\Sigma}^-$ have been predicted theoretically based on first order perturbative QCD. In the prediction of Claudson, Glashow and Wise [2], the mass of the final baryon is taken into account as a whole, while the constituent quarks inside the baryon are taken as massless when calculating the decay amplitude. In the prediction of Carimalo [3], mass effects at the quark level are taken into consideration. Experimentally, the related measurements are needed for the test. According to the helicity formalism, the angular distribution of $\psi(3686) \to B\bar{B}$ can be written as

$$dN/dcos\theta_B \propto 1 + \alpha cos^2\theta_B$$

where θ_B is the angle between the direction of the baryon and the $e^-(e^+)$ beam direction. At present, the α values have been measured for Σ baryons in Table 1. Those angular distributions reflect details of the baryon structure. Various theoretical models have predicted the values, such as Helicity Selection Rules. To explain the difference between theoretical predictions and experimental measurements, many effects are considered to correct the theoretical models, such as quark mass effects and electromagnetic effects. Unfortunately, no conclusive theoretical model has been able to explain these measured values.

Besides, Perturbative QCD [4] predicts that the partial widths for J/ψ decays into an exclusive hadronic state h are proportional to the squares of the wave-function, which are well determined from the leptonic widths. And it is also related to the strong coupling constant , which is expected to behave in the same way for the two resonances J/ψ and $\psi(3686)$. From this assumption $J/\psi \to h$ and $\psi(3686) \to h$ can be related via

$$\frac{B(\psi(3686) \to h)}{B(J/\psi \to h)} \approx \frac{B(\psi(3686) \to e^+e^-))}{B(J/\psi \to e^+e^-)} \approx 12\%$$

This relation defines the "12%rule", which works reasonably well for many specific decay modes. A large violation of this rule was observed by later experiments, particularly in $\rho\pi$ decay. Recent reviews [5] [6] of relevant theories and experiments conclude that current theoretical explanations are unsatisfactory. Clearly, more experimental results are desirable. Some branching fraction have been measured in Table 1. However, this process of $\psi(3686) \to \Sigma^-\bar{\Sigma}^+$ has never been studied. The study of baryon spectroscopy plays an important role in the development of the quark model and in the understanding of QCD.

Tab. 1: The α value and branching fraction of $J/\psi(\psi(3686))$ decay to Σ pair

Decay mode	Branching fraction($\times 10^{-4}$)	α value
$J/\psi \to \Sigma^+\bar{\Sigma}^-$	$11.50 \pm 0.10 \pm 0.22$ [7]	$-0.508 \pm 0.006 \pm 0.002$ [7]
$J/\psi \to \Sigma^0\bar{\Sigma}^0$	11.72 ± 0.32 [8]	$-0.461 \pm 0.006 \pm 0.007$ [9]
$J/\psi \to \Sigma^-\bar{\Sigma}^+$	$14.81 \pm 0.012 \pm 0.3$ [10]	$-0.355 \pm 0.003 \pm 0.007$ [10]
$\psi(3686) \to \Sigma^+\bar{\Sigma}^-$	$2.43 \pm 0.03 \pm 0.07$ [7]	$0.682 \pm 0.030 \pm 0.011$ [7]
$\psi(3686) \to \Sigma^0\bar{\Sigma}^0$	$2.44 \pm 0.03 \pm 0.11$ [8]	$0.71 \pm 0.11 \pm 0.04$ [8]
$\psi(3686) \to \Sigma^-\bar{\Sigma}^+$	Not be measured	Not be measured

2 Detector

The BESIII detector [11] records symmetric e^+e^- collisions provided by the BEPCII storage ring [12], which operates with a peak luminosity of 1×10^{33} cm^{-2}s^{-1} in the center of mass energy range from 2.0 to 4.9 GeV. BESIII has collected large data samples in this energy region [13]. The cylindrical core of the BESIII detector covers 93% of the full solid angle and consists of a helium-based multilayer drift chamber (MDC), a plastic scintillator time-of-flight system (TOF), and a CsI(Tl) electromagnetic calorimeter (EMC), which are all enclosed in a superconducting solenoidal magnet providing a 1.0 T (0.9 T in 2012) magnetic field. The solenoid is supported by an octagonal flux-return yoke with resistive plate counter muon identification modules interleaved with steel. The charged-particle momentum resolution at 1 GeV/c is 0.5%, and the dE/dx resolution is 6% for electrons from Bhabha scattering. The EMC measures photon energies with a resolution of 2.5% (5%) at 1 GeV in the barrel (end cap) region. The time resolution in the TOF barrel region is 68 ps, while that in the end cap region is 110 ps. The end cap TOF system was upgraded in 2015 using multi-gap resistive plate chamber technology, providing a time resolution of 60 ps [14].

3 Data and Monte Carlo

3.1 Data

The data sample of 448.1×10^6 $\psi(3686)$ events has been collected with the BESIII detector at the BEPCII collider during 2009 and 2012 year.

3.2 Monte Carlo Simulation and Method

The signal MC sample is generated by mDIY generator with the angular amplitude following the differential distribution function. Here θ_Σ is the angle between Σ^- and the positron (e^+) beam in the reaction center-of-mass frame. The other four angles are the polar and azimuthal angles of the π^+ and anti-neutron(or π^- and neutron) in the helicity frame, respectively. To obtain the helicity angles, one begins from the production scattering plane of $e^+e^- \to \psi(3686) \to \Sigma^-\bar{\Sigma}^+ \to n\pi^-\bar{n}\pi^+$ the system. This is obtained by considering the centre-of-mass (CM) system where the four-momenta of the electron-positron and $\Sigma^-\bar{\Sigma}^+$ are given by

$$\begin{aligned} \vec{p}_{\Sigma^-} &= -\vec{p}_{\bar{\Sigma}^+} \\ \vec{k}_{e^+} &= -\vec{k}_{e^-} = \vec{k}. \end{aligned} \tag{1}$$

The xz-scattering plane is defined by the $\vec{p}$ and $\vec{k}$ vectors and the $\vec{p}$ and $\vec{k}$ vectors are the unit vector of $\vec{\Sigma}$ and $\vec{e}$, while the y-axis is the normal to the plane. From a right-handed coordinate system with the basis vectors

$$\begin{aligned} \vec{e}_x &= \frac{1}{sin\theta_\Sigma}(\vec{p} \times \vec{k}) \times \vec{p} \\ \vec{e}_y &= \frac{1}{sin\theta_\Sigma}(\vec{p} \times \vec{k}) \\ \vec{e}_z &= \vec{p}, \end{aligned} \tag{2}$$

the helicity angles are obtained, where $\vec{p}$ and $\vec{k}$ are the unit vectors of $\vec{p}_\Sigma$ and $\vec{k}_e$, respectively. As seen from the basis vector definitions in Figure 1, the helicity angles are defined with respect to the direction of the outgoing hyperon in the CM frame ($\vec{e}_z$). Technically the helicity angles are obtained by (i) boosting the hyperon(anti-hyperon) in the CM frame and obtain the polar, $\theta^-_\Sigma(\theta_{\bar{\Sigma}^+})$ and $\phi_{\Sigma^-}(\phi_{\bar{\Sigma}^+})$, (ii) by boosting the neutron(anti-neutron) first in the CM frame and then into the hyperon(anti-hyperon) rest frame, (iii) and then by rotating the neutron(anti-neutron) with respect to the boosted z-axis and y-axis with an angle $-\phi_{\Sigma^-}(\phi_{\bar{\Sigma}^+})$ and $-\theta^-_\Sigma(\theta_{\bar{\Sigma}^+})$, respectively.

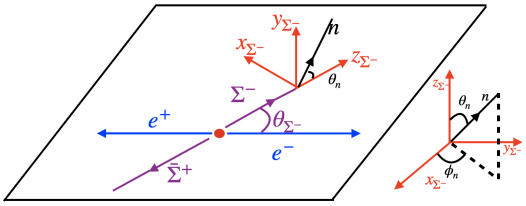

Fig. 1: the helicity frame we used in the $\psi(3686) \to \Sigma^-\bar{\Sigma}^+$,$\Sigma^- \to n\pi^-$, $\bar{\Sigma}^+ \to \bar{n}\pi^+$.

The theoretical formula [15] we used is

$$\begin{aligned} W(\xi) =& t_0(\xi) + \alpha_\psi t_5(\xi) \\ &+ \alpha\bar{\alpha}(t_1(\xi) + \sqrt{1-\alpha_\psi^2}cos(\Delta\phi)t_2(\xi) + \alpha_\psi t_6(\xi) \\ &\sqrt{1-\alpha_\psi^2}sin(\Delta\phi)(\alpha t_3(\xi) - \bar{\alpha}t_4(\xi)). \end{aligned} \tag{3}$$

The arguments to the function are

$$\begin{aligned} t_0(\xi) &= 1 \\ t_1(\xi) &= sin^2\theta sin\theta_n sin\theta_{\bar{n}} cos\phi_n cos\phi_{\bar{n}} + cos^2\theta cos\theta_n cos\theta_{\bar{n}} \\ t_2(\xi) &= sin\theta cos\theta(sin\theta_n cos\theta_{\bar{n}} cos\phi_n + cos\theta_n sin\theta_{\bar{n}} cos\phi_{\bar{n}}) \\ t_3(\xi) &= sin\theta cos\theta sin\theta_n sin\phi_n \\ t_4(\xi) &= sin\theta cos\theta sin\theta_{\bar{n}} sin\phi_{\bar{n}} \\ t_5(\xi) &= cos^2\theta \\ t_6(\xi) &= cos\theta_n cos\theta_{\bar{n}} - sin^2\theta sin\theta_n sin\theta_{\bar{n}} sin\phi_n sin\phi_{\bar{n}} \end{aligned} \tag{4}$$

In the formula (3), ξ represents the polar angle and azimuth angle of the particle in its final state, α_ψ represents the angular distribution parameter, α is equal to 0.068, and $\bar{\alpha}$ is equal to -0.068 [16]. The formula consists of three parts: the first term represents the scattering angle of the Σ particle, the second term represents the correlation of the spins, and the third term is the independent polarization term.

At the same time, we also simulate possible background events to verify and test our case selection procedures and data processing methods. Simulated samples produced with the GEANT4-based [17] Monte Carlo (MC) package which includes the geometric description of the BESIII detector and the detector response, are used to determine the detection efficiency and to estimate the backgrounds. The $\psi(3686)$ resonance is simulated with the KKMC generator [18], which is an event generator based on precise predictions of the Electroweak Standard Model for the process. The beam energy spread and initial state radiation (ISR) are taken into account in the simulation. The software framework used for the data analysis is BOSS(BESIII Offline Software System), which is developed from Gaudi. This work is

under BOSS version 6.6.4p03. About $(448.1\pm2.9)\times10^6$ $\psi(3686)$ MC inclusive events for $\psi(3686)$ is used to investigate possible backgrounds.The known decay modes are modelled with EVTGEN [19] using branching fractions taken from the Particle Data Group [16], and the remaining unknown charmonium decays are modelled with LUNDCHARM [20]. Final state radiation (FSR) from charged final state particles is incorporated using the PHOTOS package.

3.3 Decay chain

In this analysis, the concerned decay channel is $\psi(3686) \rightarrow \Sigma^-\bar{\Sigma}^+$, where $\Sigma^-/\bar{\Sigma}^+$ is reconstructed from $n\pi^-(\bar{n}\pi^+)$.

4 Event Selection of $\psi(3686) \to \Sigma^-\bar{\Sigma}^+, \Sigma^- \to n\pi^-, \bar{\Sigma}^+ \to \bar{n}\pi^+$

4.1 Track Level Selection

Charged tracks reconstructed by main drift chamber(MDC) hit information must be fitted by Kalman method successfully and come from the interaction region in three dimensions. Due to changing beam conditions, the interaction point (IP) moves. Thus, a separate average IP is determined for each run using the VertexDbSvc package. The Σ^- particle has a longer life time, so it requires a wider distance and the reference we refer to is [10]. Relative to this run-dependent IP, each charged track must satisfy the following requirements:

- $V_{xy} < 10$ cm,
- $|V_z| < 30$ cm,
- $|\cos\theta| < 0.93$,
- Good track is required $N = 2$ and total charge is equal to 0.

Here, θ is the polar angle of the charged track with respect to the beam axis, V_{xy} and $|V_z|$ are the closest approaches of a charged track to the interaction point in the Oxy plane and in the z position.

4.2 Particle identification

The charged pions are identified via ParticleID package by using the TOF and dE/dx measurements with which the combined confidence levels $\mathscr{L}(\pi)$, $\mathscr{L}(p)$ and $\mathscr{L}(K)$ for pion, proton and kaon hypotheses are calculated, respectively. The particle is considered to be $\pi^-(\pi^+)$ if the $Prob_{PID}$ greater than any other particle hypothesis. We require the π^+ and π^- candidates satisfy the following criteria:

- $\pi^\pm$: $\mathscr{L}(\pi) > \mathscr{L}(p)$ and $\mathscr{L}(\pi) > \mathscr{L}(K)$,

4.3 $\bar{n}$ Shower Requirement

For the anti-neutron selection, the good anti-neutron can be selected by using the most energy. For the neutron selection, it is not easy to select neutron because the neutron shower is similar as gamma shower in EMC. The cluster in the EMC which satisfies the following criteria is regarded as a good $\bar{n}$ shower:

- barrel EMC, $|\cos\theta| < 0.80$; endcap EMC, $0.86 < |\cos\theta| < 0.92$;
- At least one shower with energy larger than 0.6 GeV is required. Fig. 2 shows the deposit energy distribution of $\bar{n}$ and n in the EMC from MC simulation.

- Second moment> 20, the reference we refer to is [21] [22](This selection is already one of the standard criteria for the selection of antineutron). The second momentum is defined as $\sum_i E_i r_i^2 / \sum_i E_i$, where E_i is the deposit energy in the i_{th} crystal and r_i is the radial distance of the crystal i from the cluster center.

- To suppress electronic noise and showers unrelated to the event, the difference between the EMC time and the event start time is required to be within (0, 700) ns

- To exclude showers that originate from charged tracks, the angle between the position of each shower in the EMC and the closest extrapolated charged track must be greater than 10 degrees and any two showers can not form π^0 candidate.

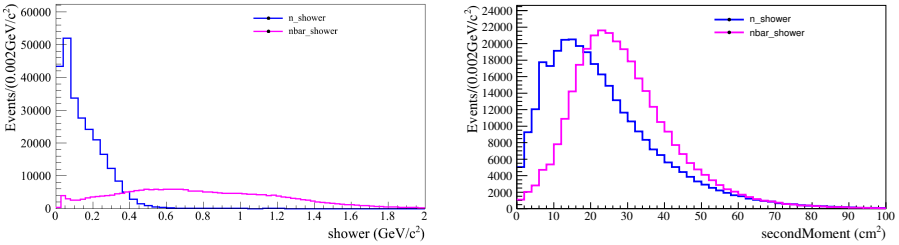

Fig. 2: Left:Deposit energy distribution in EMC from MC simulation. The distribution indicates that E_n is less than 0.6 GeV/c^2. So for $\bar{n}$ selection, the energy for the most energetic shower is required larger than 0.6 GeV. Right:The distributions of the secondmoment for neutron and anti-neutron.

4.4 $M_{rec(\pi^+\pi^-)}$ mass window

The events of signal mc are produced according to our estimated branching ratio, and the events of background come from inclusive mc, as Fig. 3. To further remove potential backgrounds and improve the mass resolution, $\psi(3686) \to \pi^+\pi^- J/\psi$ background and other background need to be suppressed, so we require $M_{rec(\pi^+\pi^-)}$ <2.9 GeV.

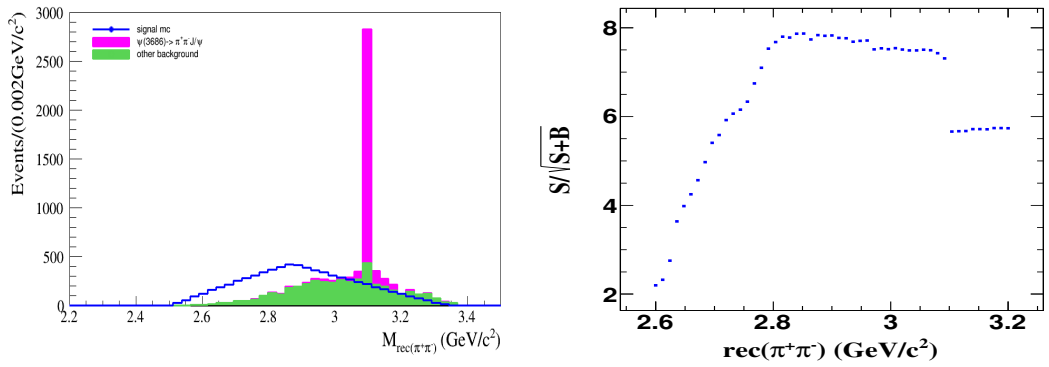

Fig. 3: Left: The figure of $M_{rec(\pi^+\pi^-)}$ invariant mass. Blue line is signal MC. Red line and green line are the backgrounds from the inclusive MC. Right: The figure is for $\psi(3686) \to \Sigma^-\bar{\Sigma}^+, \Sigma^- \to n\pi^-, \bar{\Sigma}^+ \to \bar{n}\pi^+$, where S is signal MC, and B is the backgrounds from the inclusive MC.

4.5 kinematic fit

To further remove potential backgrounds and to improve the mass resolution, the kinematic fit (1C fit) is performed. In the kinematic fit, we require the four momentum conservation and the invariant mass of M($\bar{n}\pi^+$) is fixed to the $\bar{\Sigma}^-$ mass($1.197GeV/c^2$). The three momentum of the neutron is missing and the energy of $\bar{n}$ is missing. Therefore, the constraints of kinematic fit is $(4 + 1 - 3 - 1) = 1C$. The resonance Σ^- is reconstructed from π^-, a charged track with full four momentum information and n, a missing neutron track. The resonance $\bar{\Sigma}^+$ is reconstructed from π^+, a charged track with full momentum information and $\bar{n}$, a neutral track with missing energy information in EMC.

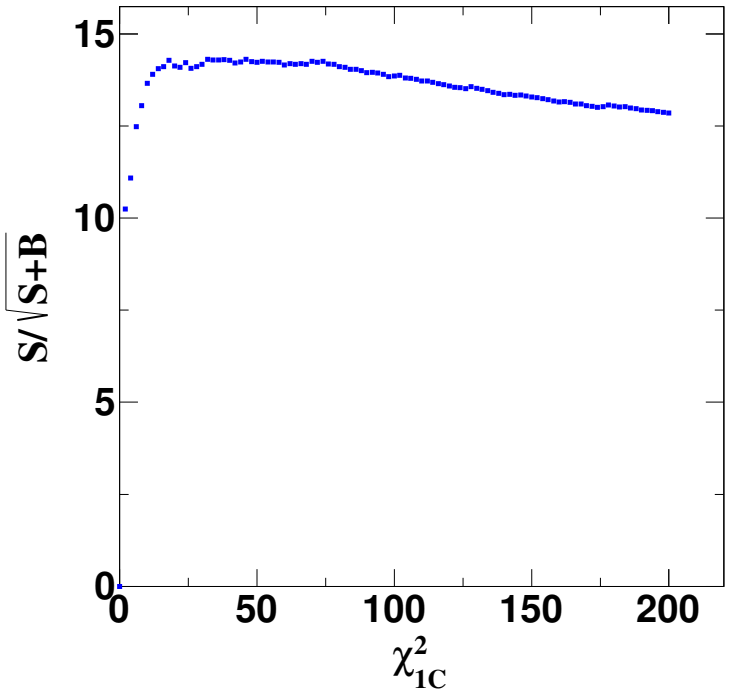

Fig. 4: Figure of kinematic fitting for the χ^2_{1C} , the figure is for $\psi(3686) \to \Sigma^-\bar{\Sigma}^+, \Sigma^- \to n\pi^-, \bar{\Sigma}^+ \to \bar{n}\pi^+$, where S is signal MC, and B is the backgrounds from the inclusive MC.

The goodness of fit quality χ^2 is required to be smaller than 50 for the decay process. This value is optimized via the figure of merit as the Fig. 4. In the picture, S is signal MC and B is the backgrounds from the inclusive MC.

4.6 Background analysis

We use $\psi(3686)$ inclusive samples to study background level. There are 597 events which pass the event selections, and the number of background events is 393. The background level is 66%. And considering in inclusive MC samples, some peaking backgrounds are not well generated. We generate these peaking decay channels.

The detail background channels could be found in Fig. 5.

No.	decay chain	final states	iTopo	nEvt	nTot
0	$\psi' \to \Sigma^+\Sigma^-$, $\Sigma^+ \to n\pi^+$, $\Sigma^- \to \pi^- n$	$\psi' \to n\pi^+\pi^- n$	1	204	204
1	$\psi' \to \Delta^-\pi^0\Delta^-$, $\Delta^- \to n\pi^+$, $\Delta^- \to \pi^- n$	$\psi' \to n\pi^+\pi^0\pi^- n$	4	53	257
2	$\psi' \to \bar{\Delta}^-\Delta^-$, $\bar{\Delta}^- \to n\pi^+$, $\Delta^- \to \pi^- n$	$\psi' \to n\pi^+\pi^- n$	0	39	296
3	$\psi' \to \bar{\Delta}^-\pi^- n$, $\bar{\Delta}^- \to n\pi^+$	$\psi' \to n\pi^+\pi^- n$	33	13	309
4	$\psi' \to \pi^0\pi^0 J/\psi$, $J/\psi \to \bar{\Delta}^-\pi^- n$, $\bar{\Delta}^- \to n\pi^+$	$\psi' \to n\pi^+\pi^0\pi^0\pi^- n$	7	10	319
5	$\psi' \to \gamma\chi_{c2}$, $\chi_{c2} \to \gamma J/\psi$, $J/\psi \to \bar{\Delta}^-\pi^- n$, $\bar{\Delta}^- \to n\pi^+$	$\psi' \to \gamma\gamma n\pi^+\pi^- n$	26	9	328
6	$\psi' \to \pi^0\pi^0 J/\psi$, $J/\psi \to n\pi^+\bar{\Delta}^-$, $\bar{\Delta}^- \to \pi^- n$	$\psi' \to n\pi^+\pi^0\pi^0\pi^- n$	13	9	337
7	$\psi' \to \gamma\chi_{c1}$, $\chi_{c1} \to \gamma J/\psi$, $J/\psi \to \bar{\Delta}^-\pi^- n$, $\bar{\Delta}^- \to n\pi^+$	$\psi' \to \gamma\gamma n\pi^+\pi^- n$	39	8	345
8	$\psi' \to \gamma\chi_{c1}$, $\chi_{c1} \to \gamma J/\psi$, $J/\psi \to n\pi^+\bar{\Delta}^-$, $\bar{\Delta}^- \to \pi^- n$	$\psi' \to \gamma\gamma n\pi^+\pi^- n$	55	8	353
9	$\psi' \to n\pi^+\bar{\Delta}^-$, $\bar{\Delta}^- \to \pi^- n$	$\psi' \to n\pi^+\pi^- n$	27	7	360
10	$\psi' \to \pi^0\pi^0 J/\psi$, $J/\psi \to n\pi^-\pi^+ n$	$\psi' \to n\pi^+\pi^0\pi^0\pi^- n$	32	7	367
11	$\psi' \to \bar{\Sigma}^+\pi^0\Sigma^-$, $\bar{\Sigma}^+ \to n\pi^+$, $\Sigma^- \to \pi^- n$	$\psi' \to n\pi^+\pi^0\pi^- n$	6	7	374
12	$\psi' \to \gamma\chi_{c1}$, $\chi_{c1} \to \bar{\Sigma}^+\pi^-\Sigma^0$, $\bar{\Sigma}^+ \to n\pi^+$, $\Sigma^0 \to \gamma\Lambda$, $\Lambda \to \pi^0 n$	$\psi' \to \gamma\gamma n\pi^+\pi^0\pi^- n$	35	7	381
13	$\psi' \to \bar{\Delta}^-\pi^-\Delta^0$, $\bar{\Delta}^- \to n\pi^+$, $\Delta^0 \to \pi^0 n$	$\psi' \to n\pi^+\pi^0\pi^- n$	15	7	388
14	$\psi' \to \gamma\chi_{c2}$, $\chi_{c2} \to n\pi^-\pi^+ n$	$\psi' \to \gamma n\pi^+\pi^- n$	8	7	395
15	$\psi' \to \gamma\chi_{c1}$, $\chi_{c1} \to \gamma J/\psi$, $J/\psi \to n\pi^-\pi^+ n$	$\psi' \to \gamma\gamma n\pi^+\pi^- n$	48	6	401
16	$\psi' \to \gamma\chi_{c0}$, $\chi_{c0} \to n\pi^-\pi^+ n$	$\psi' \to \gamma n\pi^+\pi^- n$	9	6	407
17	$\psi' \to \eta J/\psi$, $\eta \to \gamma\gamma$, $J/\psi \to \bar{\Delta}^-\Delta^-$, $\bar{\Delta}^- \to n\pi^+$, $\Delta^- \to \pi^- n$	$\psi' \to \gamma\gamma n\pi^+\pi^- n$	22	5	412
18	$\psi' \to \pi^0\pi^0 J/\psi$, $J/\psi \to \bar{\Delta}^-\Delta^-$, $\bar{\Delta}^- \to n\pi^+$, $\Delta^- \to \pi^- n$	$\psi' \to n\pi^+\pi^0\pi^- n$	12	5	417
19	$\psi' \to \gamma\chi_{c0}$, $\chi_{c0} \to \bar{\Delta}^-\pi^- n$, $\bar{\Delta}^- \to n\pi^+$	$\psi' \to \gamma n\pi^+\pi^- n$	19	5	422
20	$\psi' \to \gamma\chi_{c1}$, $\chi_{c1} \to \gamma J/\psi$, $J/\psi \to \bar{\Delta}^-\Delta^-$, $\bar{\Delta}^- \to n\pi^+$, $\Delta^- \to \pi^- n$	$\psi' \to \gamma\gamma n\pi^+\pi^- n$	57	5	427
21	$\psi' \to \gamma\chi_{c0}$, $\chi_{c0} \to \bar{\Sigma}^+\pi^-\Sigma^0$, $\bar{\Sigma}^+ \to n\pi^+$, $\Sigma^0 \to \gamma\Lambda$, $\Lambda \to \pi^0 n$	$\psi' \to \gamma\gamma n\pi^+\pi^0\pi^- n$	61	5	432
22	$\psi' \to \eta J/\psi$, $\eta \to \gamma\gamma$, $J/\psi \to \bar{\Delta}^-\pi^- n$, $\bar{\Delta}^- \to n\pi^+$	$\psi' \to \gamma\gamma n\pi^+\pi^- n$	69	5	437
23	$\psi' \to \gamma\chi_{c2}$, $\chi_{c2} \to \gamma J/\psi$, $J/\psi \to \bar{\Delta}^-\Delta^-$, $\bar{\Delta}^- \to n\pi^+$, $\Delta^- \to \pi^- n$	$\psi' \to \gamma\gamma n\pi^+\pi^- n$	78	5	442
24	$\psi' \to \gamma\chi_{c0}$, $\chi_{c0} \to \bar{\Sigma}^+\pi^-\Lambda$, $\bar{\Sigma}^+ \to n\pi^+$, $\Lambda \to \pi^0 n$	$\psi' \to \gamma n\pi^+\pi^0\pi^- n$	50	4	446
25	$\psi' \to \gamma\chi_{c1}$, $\chi_{c1} \to n\pi^-\pi^+ n$	$\psi' \to \gamma n\pi^+\pi^- n$	51	4	450
26	$\psi' \to \gamma\chi_{c1}$, $\chi_{c1} \to \bar{\Delta}^-\pi^- n$, $\bar{\Delta}^- \to n\pi^+$	$\psi' \to \gamma n\pi^+\pi^- n$	10	4	454
27	$\psi' \to \eta J/\psi$, $\eta \to \gamma\gamma$, $J/\psi \to n\pi^-\pi^+ n$	$\psi' \to \gamma\gamma n\pi^+\pi^- n$	18	4	458
28	$\psi' \to \gamma\chi_{c1}$, $\chi_{c1} \to \bar{\Delta}^-\pi^-\Delta^0$, $\bar{\Delta}^- \to n\pi^+$, $\Delta^0 \to \pi^0 n$	$\psi' \to \gamma n\pi^+\pi^0\pi^- n$	29	4	462
29	$\psi' \to \bar{\Sigma}^+ K^{*-} n$, $\bar{\Sigma}^+ \to n\pi^+$, $K^{*-} \to \pi^- K_L$	$\psi' \to n\pi^+ K_L\pi^- n$	44	4	466
30	$\psi' \to \gamma\chi_{c1}$, $\chi_{c1} \to \Delta^0\pi^+\bar{\Delta}^-$, $\Delta^0 \to n\pi^0$, $\bar{\Delta}^- \to \pi^- n$	$\psi' \to \gamma n\pi^+\pi^0\pi^- n$	25	4	470
31	$\psi' \to \gamma\chi_{c0}$, $\chi_{c0} \to n\pi^+\bar{\Delta}^-$, $\bar{\Delta}^- \to \pi^- n$	$\psi' \to \gamma n\pi^+\pi^- n$	40	3	473
32	$\psi' \to \gamma\chi_{c0}$, $\chi_{c0} \to \bar{\Delta}^0\pi^+\Delta^-$, $\bar{\Delta}^0 \to n\pi^0$, $\Delta^- \to \pi^- n$	$\psi' \to \gamma n\pi^+\pi^0\pi^- n$	3	3	476
33	$\psi' \to \pi^-\pi^+ J/\psi$, $J/\psi \to \bar{\Delta}^-\Delta^-$, $\bar{\Delta}^- \to n\pi^+$, $\Delta^- \to \pi^- n$	$\psi' \to n\pi^+\pi^+\pi^-\pi^- n$	21	3	479

Fig. 5: Topology of $\psi(3686) \to \Sigma^-\bar{\Sigma}^+$ in generic $\psi(3686)$ inclusive MC sample.

We draw main background and signal events based on the $\psi(3686)$ inclusive samples in the Fig. 6. Three dominant peaking background channels are shown in Table 2. Because the background description of the inclusive mc is not necessarily reliable, the branching fraction of three peaking background channels $\psi(3686) \to \gamma\Sigma^-\bar{\Sigma}^+$, $\psi(3686) \to \pi^0\Sigma^-\bar{\Sigma}^+$, $\psi(3686) \to \gamma\eta_c(\eta_c \to \Sigma^-\bar{\Sigma}^+)$ have been estimated by using decay channels of $\psi(3686) \to \gamma\Sigma^+\bar{\Sigma}^-$, $\psi(3686) \to \pi^0\Sigma^+\bar{\Sigma}^-$, $\psi(3686) \to \gamma\eta_c(\eta_c \to \Sigma^+\bar{\Sigma}^-)$. The background events of $\psi(3686) \to \gamma\Sigma^-\bar{\Sigma}^+$ and $\psi(3686) \to \gamma\eta_c(\eta_c \to \Sigma^+\bar{\Sigma}^-)$ is 320±53 and 5±1, which will contribute as peaking background when we fit the real data.

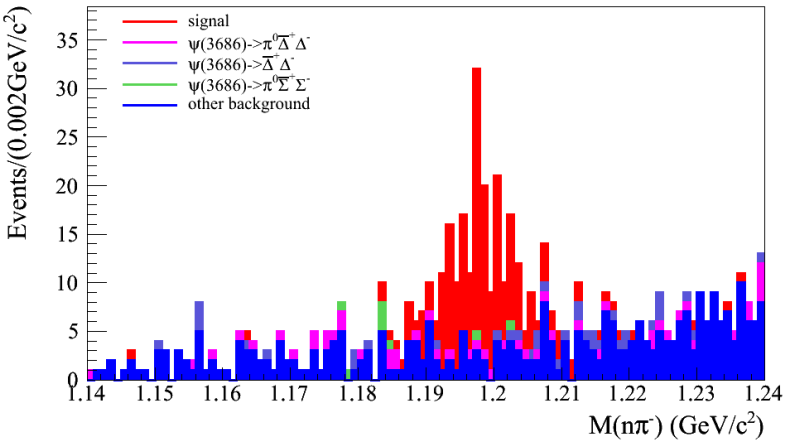

Fig. 6: Background distribution of $\psi(3686)$ inclusive MC sample.

Tab. 2: The number of events of main peaking background

Channel	Branching fraction	ε_{MC}	number of events
$\psi(3686) \to \gamma\Sigma^-\bar{\Sigma}^+$	$(1.2 \pm 0.2) \times 10^{-4}$(Appendix.E)	0.595%	320 ± 53
$\psi(3686) \to \pi^0\Sigma^-\bar{\Sigma}^+$	$(1.8 \pm 0.4) \times 10^{-6}$(refer [28])	0.203%	ignorable
$\psi(3686) \to \gamma\eta_c, \eta_c \to \Sigma^-\bar{\Sigma}^+$	$(3.4 \pm 0.05) \times 10^{-3} \times (2.1 \pm 0.6) \times 10^{-3}(PDG)$	0.186%	5 ± 1

5 Decay Measurement

5.1 MC efficiency

To extract decay parameters from the decay channels of $\psi(3686) \to \Sigma^-\bar{\Sigma}^+(\Sigma^- \to n\pi^-, \bar{\Sigma}^+ \to \bar{n}\pi^+)$, the detection efficiency should be considered. When we generate the phase space MC sample, we take the detection efficiency difference between data and MC into account. Since the final states are $\bar{n}$, π^+ and π^-, we compare the detection efficiencies of these particle between MC and real data. By selecting the control samples (the details in Appendix), the efficiencies are compared in different transverse momenta and polar angles for $\bar{n}$ [23], π^+ and π^- [24] in Fig. 7 to Fig. 9. If $\bar{n}$ momenta $\geqslant$ 1.2 GeV, we will use $\psi(3686) \to p\bar{n}\pi^-$ because the $\bar{n}$ momenta can not reach 1.2 GeV in decay channel of $J/\psi \to p\bar{n}\pi^-$ and the difference of efficiencies are only compared in different transverse momenta because the total amount of $\psi(3686)$ data is not enough in the right Fig. 7.

In order to correct the detection efficiency to real data, we did in the following steps. Firstly, for each event, the efficiency ratio between data and MC could be calculated by:

$$r_\epsilon = \frac{\epsilon^{data}_{\pi^+} \times \epsilon^{data}_{\pi^-} \times \epsilon^{data}_{\bar{n}}}{\epsilon^{MC}_{\pi^+} \times \epsilon^{MC}_{\pi^-} \times \epsilon^{MC}_{\bar{n}}}, (\Sigma^- \to n\pi^-, \bar{\Sigma}^+ \to \bar{n}\pi^+)$$

.

where represent the efficiency for this events corresponding to the different transverse momentum, energy region and polar angle. The superscripts delegate the efficiencies in real data and MC.

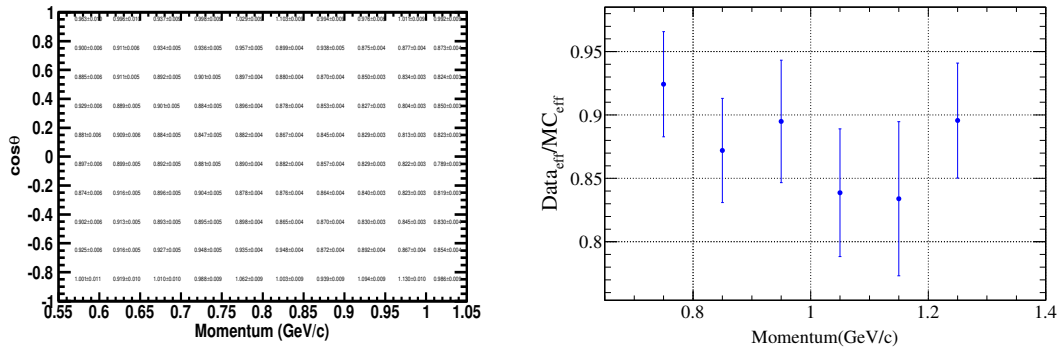

Fig. 7: Left: The ratio of Data-MC for $\bar{n}$ efficiency in terms of cosθ in different momentum range by using control sample $J/\psi \to p\bar{n}\pi^-$. Right: The ratio of Data-MC for $\bar{n}$ selection efficiency in different energy deposition in EMC(0.8-1.4GeV) by using control sample $\psi(3686) \to p\bar{n}\pi^-$.

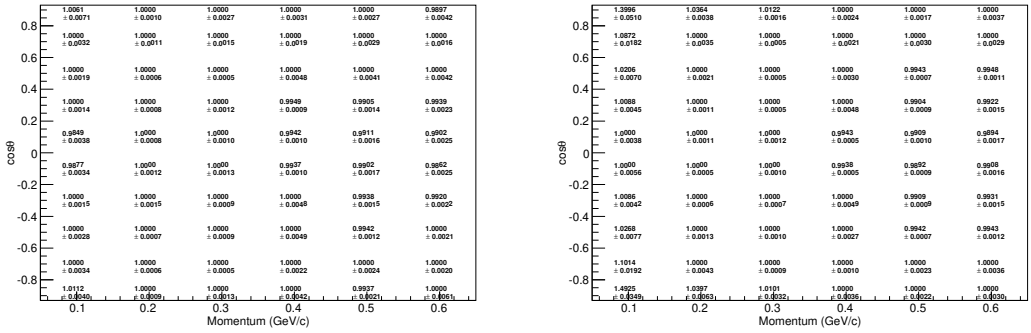

Fig. 8: The ratio of Data-MC for π^- efficiency in terms of cosθ in different momentum range by using control sample $J/\psi \to p\bar{p}\pi^+\pi^-$(left: 2009 year, right: 2012 year).

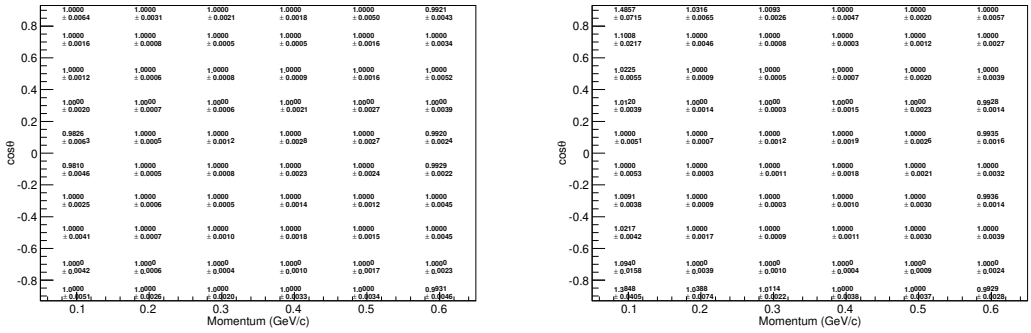

Fig. 9: The ratio of Data-MC for π^+ efficiency in terms of cosθ in different momentum range by using control sample $J/\psi \to p\bar{p}\pi^+\pi^-$(left: 2009 year, right: 2012 year).

In order to correct the detection efficiency to real data, we did in the following steps. For the case $r_\epsilon < 1$, a random number η within (0,1) is generated, if $\eta < r_\epsilon$, this event is accepted. If not, this event is rejected. For another case $r_\epsilon > 1$, this event is accepted. To increase the correction procedure, when $r_\epsilon > 1$, we also generate a random number η within (0,1). If $r_\epsilon - 1 > \eta$, this event is accepted twice. By looping all signal MC events, we could get a new MC sample which the efficiency is corrected to the real data.

5.2 α value results

The angular distributions for Σ^+ are shown, which are distributed like $1 + \alpha cos^2\theta$ as well know baryon angular distributions. The selection efficiency curve is described by this forumula: $\epsilon(\theta_\Sigma) = a_0 \times (1 + a_1 \times cos^2\theta_\Sigma + +a_2 \times cos^4\theta_\Sigma + a_3 \times cos^6\theta_\Sigma + a_4 \times cos^8\theta_\Sigma)$ in Fig. 10.

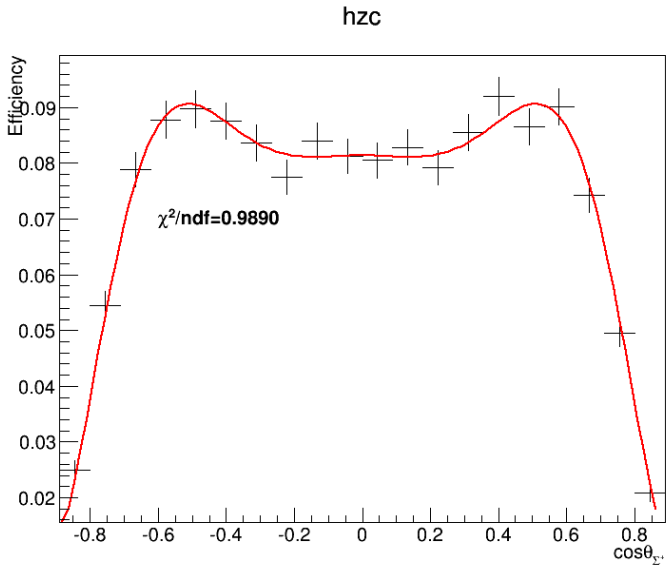

Fig. 10: The selection efficiency in different cosθ value.

To consider the influence of background, the cosine of angles are divided into 10 intervals from -1 to 1. The signal is described by the MC shape convoluted with Gaussian function which represents the difference between data and MC in the resolution and mean value. The background is described with 2nd order polynomial function, as Fig. 11.

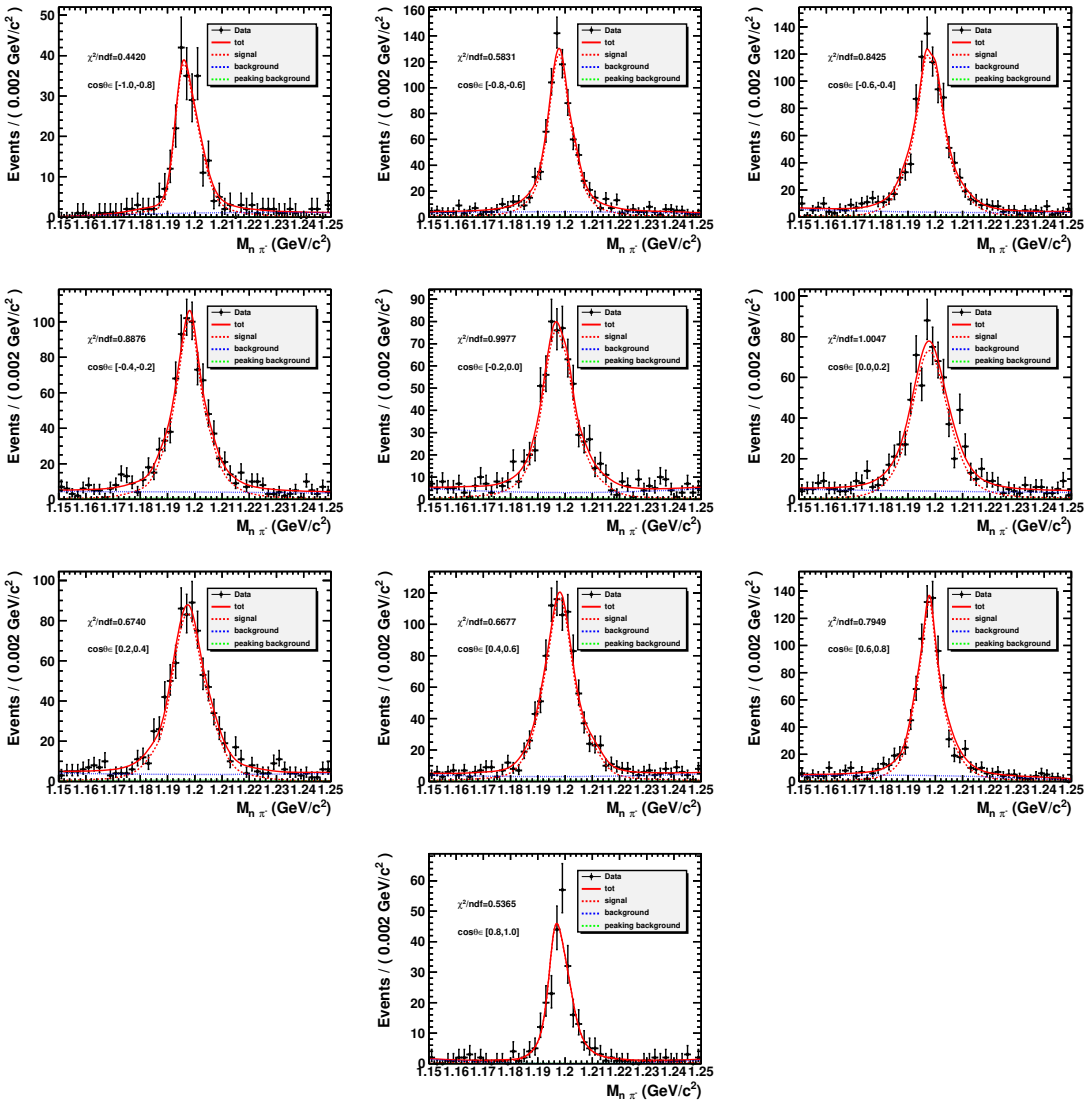

Fig. 11: The fitting of Σ^- invariant mass in each cosθ interval.

The angular distributions for $\psi(3686) \to \Sigma^-\bar{\Sigma}^+$ can be measured by fitting with

$$dN/dcos\theta_\Sigma \propto (1 + \alpha cos^2\theta_\Sigma) \times \epsilon(\theta_\Sigma), \tag{5}$$

where θ_Σ is the polar angle of Σ^- in $\psi(3686)$ CM frame, and α is the angular distribution parameter. To suppress influence of background, the events of every bin are determined by fitting real data in the Fig. 11. The fitting results is shown in the Fig. 12. The decay parameter α is measured to be 0.964 ± 0.091 for the first time.

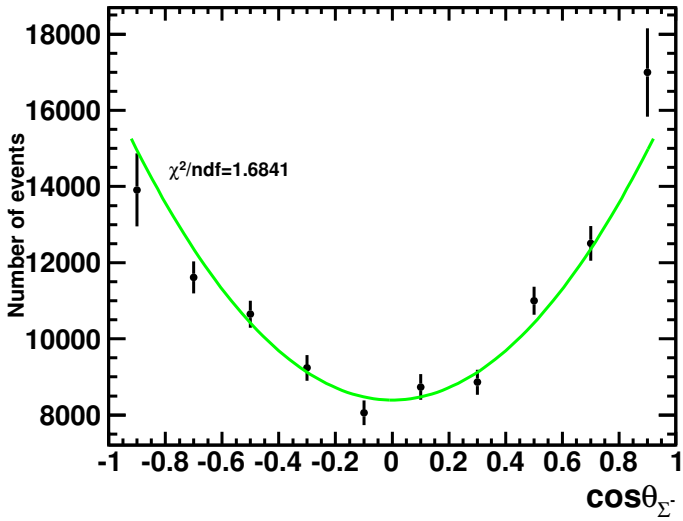

Fig. 12: The fitting results of the angular distribution(10 bins in $\cos\theta_{\Sigma^-}$).

6 Branching Results

The branch fraction is calculated according to

$$\begin{aligned} Br &= \frac{N_{sig}(X)}{\varepsilon(X) \times \prod Br_i \times N_{tot}} = \frac{N_{sig} - N_{QED}}{\varepsilon_{cor} \times 0.99848 \times 0.99848 \times 448.1 \times 10^6}, \\ &= \frac{6751 - 92}{5.26\% \times 0.99848 \times 0.99848 \times 448.1 \times 10^6} = 2.83 \times 10^{-4} \end{aligned} \tag{6}$$

where X represents $\Sigma^- \to n\pi^-$ ($\bar{\Sigma}^+ \to \bar{n}\pi^+$), $N_{sig}(X)$ is the signal events by fitting method, $\varepsilon(X)$ is the detection efficiency determined by MC which is generated according to the decay parameters measured in the real data, $\prod Br_i$ is the product branching fractions of all the intermediate states in each channel, N_{tot} is the total number of $\psi(3686)$ events.

6.1 Branching Ratio of $\psi(3686) \to \Sigma^-\bar{\Sigma}^+$

To yield the signal events, the fitting of the invariant mass of n and π^- is performed in the region of [1.15, 1.25] GeV, by requiring that the signal region of $\bar{\Sigma}^+$ fixed in 1.197 GeV. The signal is described by the MC shape convoluted with Gaussian function which represents the difference between data and MC in the resolution and mean value. The peaking background is fixed in shape and events in Table 2. The background is described with 2nd order polynomial function, as Fig. 13. Besides, we have considered QED backgrounds in 3.65GeV. The fitting results, ε_{MC}(selection efficiency) and ε_{cor}(selection efficiency after considering mc efficiency correction) are listed in the Tab. 3, and the branching fractions is measured to be $(2.83 \pm 0.04) \times 10^{-4}$. Here, we need to consider the efficiency difference between data and MC, which include the detection efficiencies of π^+, π^-, and $\bar{n}$.

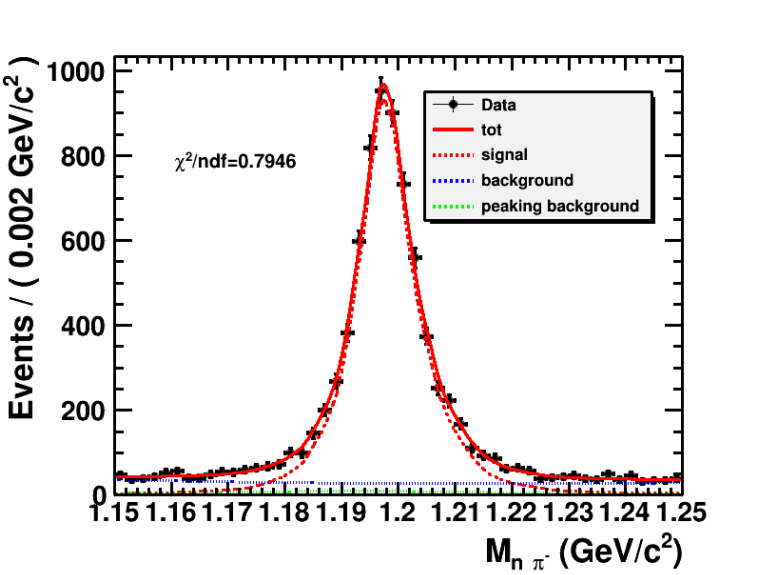

Fig. 13: The fitting of Σ^- invariant mass.

Tab. 3: The event number of $\psi(3686)$ data

Channel	N_{sig}	N_{QEDbkg}	ε_{MC}	ε_{cor}
$\psi(3686) \to \Sigma^-\bar{\Sigma}^+$	6751 ± 103	105 ± 60	6.02%	5.26%

7 Systematic uncertainty

The systematic uncertainties of the angular distribution and branching fractions are studied separately.

7.1 Systematic uncertainties of angular distribution

The systematic uncertainties of decay parameters consist of MC efficiency correction uncertainties, fitting method, kinematic fitting and signal mass window. They are listed in the Table 13

7.1.1 MC efficiency correction

The uncertainties of the MC efficiency correction is studied by considering the efficiency difference between MC and real data or not. In the Section 5.1, we compared the efficiency difference between MC and real data. We take the difference between the maximum error bar of the correction factor and the normal correction as the systematic uncertainties. The results are listed in the Table 4.

Tab. 4: The systematic uncertainty of mc efficiency correction

Decay Parameters	with	without	difference
$\alpha_{\psi(3686)}$	0.964 ± 0.091	0.969 ± 0.091	0.005

Tab. 5: The systematic uncertainty of $M_{rec(\pi^+\pi^-)}$.

Decay Parameters	norminal	Barlow method	maximum difference
$\alpha_{\psi(3686)}$	0.964 ± 0.091	0.952 ± 0.089	0.012

7.1.2 QED peaking background estimation

To estimate the uncertainties of QED background events, changing QED background events in 1σ range, its' contribution is negligible.

7.1.3 Non-peaking background estimation estimation

To estimate the uncertainties of background events, we changed the order of polynomial functions for background descriptions. The differences are taken as the systematic uncertainties comparing the nominal values, 0.8% for $\psi(3686) \to \Sigma^-\bar{\Sigma}^+$. The results are listed in the Table 6.

Tab. 6: The systematic uncertainty of fitting range

Decay Parameters	with	without	difference
$\alpha_{\psi(3686)}$	0.964 ± 0.091	0.997 ± 0.109	0.033

7.1.4 Peaking background estimation

For the peaking background, we change the normalized numbers of fixed peaking background events in 1σ. The fitting results are listed in the following Table 7, and take the difference with the nominal values as the uncertainties.

Tab. 7: The systematic uncertainty of peaking background.

Decay Parameters	norminal	$-\sigma$	$+\sigma$	difference
$\alpha_{\psi(3686)}$	0.964 ± 0.091	0.978 ± 0.114	0.965 ± 0.112	0.014

7.1.5 Kinematic fitting

With the track correction for the helix parameters, the χ^2_{1C} distribution should be more consistent between data and MC in the Fig. 14. Then we could use the difference between before correction and after correction as the systematic uncertainties, and take the values with correction as the nominal one. The results with the helix parameters are listed in the Table 8.

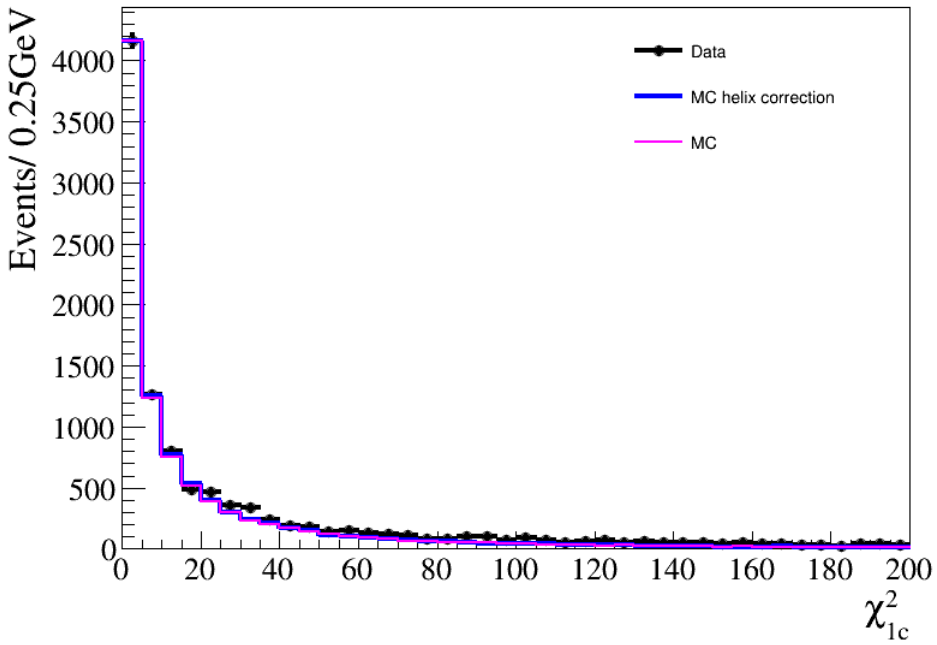

Fig. 14: The χ^2_{1c} distribution for $\psi(3686) \to \Sigma^-\bar{\Sigma}^+$.

Tab. 8: The systematic uncertainty of kinematic fitting.

Decay Parameters	with	without	difference
$\alpha_{\psi(3686)}$	0.964 ± 0.091	0.957 ± 0.101	0.025

7.1.6 Number of $\cos\theta$ bins

Instead of the 10 intervals, we use the 8 intervals to fit data. The fitting results are listed in the following Table 9, and take the difference with the nominal values as the uncertainties.

Tab. 9: The systematic uncertainty of cosθ bin.

Decay Parameters	norminal(10 bin)	8 bin	difference
$\alpha_{\psi(3686)}$	0.964 ± 0.091	0.968 ± 0.089	0.004

7.1.7 Fitting $\cos\theta$ range

After varying cosθ fitting range from [-1.0, 1.0] to [-0.8, 0.8], the fitting results are listed in the following Table 10, and take the difference with the nominal values as the uncertainties.

Tab. 10: The systematic uncertainty of fitting range.

Decay Parameters	norminal	smaller interval	difference
$\alpha_{\psi(3686)}$	0.964 ± 0.091	0.945 ± 0.105	0.019

7.1.8 Summary of α parameter uncertainties

All the sources of systematic uncertainties are treated as uncorrelated and summed in quadrature, listed in Table 11.

Tab. 11: The total uncertainties of the α value for $\Sigma^- \to n\pi^-, \bar{\Sigma}^+ \to \bar{n}\pi^+$

Systematic error	$\alpha_{\psi(3686)}$
MC efficiency correction	0.005
QED peaking Background estimation	negligible
Non-Peaking Background estimation	0.012
Peaking background estimation	0.014
Kinematic fitting	0.003
Number of $\cos\theta$ bin	0.004
Fitting $\cos\theta$ range	0.019
Total	0.029

7.2 Systematic uncertainties of branching fraction measurement

The uncertainties of the branching fraction measurement include the uncertainties of MC efficiency correction, the uncertainties of decay parameters, the fitting range, signal shape, background estimation, kinematic fitting, total number of $\psi(3686)$ events and $\bar{n}$ correction, which are listed in the Tab 12.

Tab. 12: The total uncertainties of the branching fraction for $\psi(3686) \to \Sigma^-\bar{\Sigma}^+$

Source	$\psi(3686) \to \Sigma^-\bar{\Sigma}^+, \Sigma^- \to n\pi^-, \bar{\Sigma}^+ \to \bar{n}\pi^+$
MC efficiency correction	1.9%
Decay parameters	1.2%
QED background estimation	0.8%
Non-Background estimation	0.8%
Peaking background estimation	0.4%
Kinematic fitting	0.2%
Total number	0.7%
Total	2.6%

7.2.1 MC efficiency correction

The differences of detection efficiencies for π^+ and π^- between data and MC have been corrected according to momentums and polar angles. The uncertainties for these correction are estimated by the following formula:

$$\Delta^2 = \sum_{i=0}^{n} \left(\frac{\epsilon_i - \epsilon_0}{\epsilon_0} \right)^2$$

where n the number of bins in different momentums and polar angles, ϵ_0 is the nominal value of efficiency, and ϵ_i is the efficiency when we change the correction factor in 1 σ for i bin. The uncertainties of π^+ and π^- tracking and PID efficiencies are estimated to 0.2% for $\psi(3686) \to \Sigma^-\bar{\Sigma}^+$. To study systematic uncertainties $\bar{n}$ efficiency correction, The differences between MC and Data have been determined by using control sample $J/\psi(\psi(3686)) \to p\bar{n}\pi^-$. We take the difference between the maximum error bar of the correction factor and the normal correction as the systematic uncertainties. The maximum difference as the systematic uncertainties, which are 1.9 % for $\psi(3686) \to \Sigma^-\bar{\Sigma}^+$, respectively.

7.2.2 Decay parameters

The efficiency is calculated based on the MC sample which is generated with decay parameters. The polarization of $\psi(3686) \to \Sigma^-\bar{\Sigma}^+$ is not measured before. When the value of $\Delta\phi$ is $-\pi/2$, 0 and $\pi/2$ by using theoretical formula 3, the efficiency of the signal MC sample is 6.05 %, 6.08 %, 6.09 %. The maximum difference as the systematic uncertainties, which are 1.2 % for $\psi(3686) \to \Sigma^-\bar{\Sigma}^+$, respectively.

7.2.3 $M_{rec(\pi^+\pi^-)}$

When the value of $M_{rec(\pi^+\pi^-)}$ is changed from 2.98 GeV/c^2 to 2.91 GeV/c^2(1-20 MeV), we compare the branching fractions with the nominal values using Barlow method and take difference as the systematic uncertainties, which is negligible for $\psi(3686) \to \Sigma^-\bar{\Sigma}^+$, respectively. The fitting results are listed in the following Fig. 15.

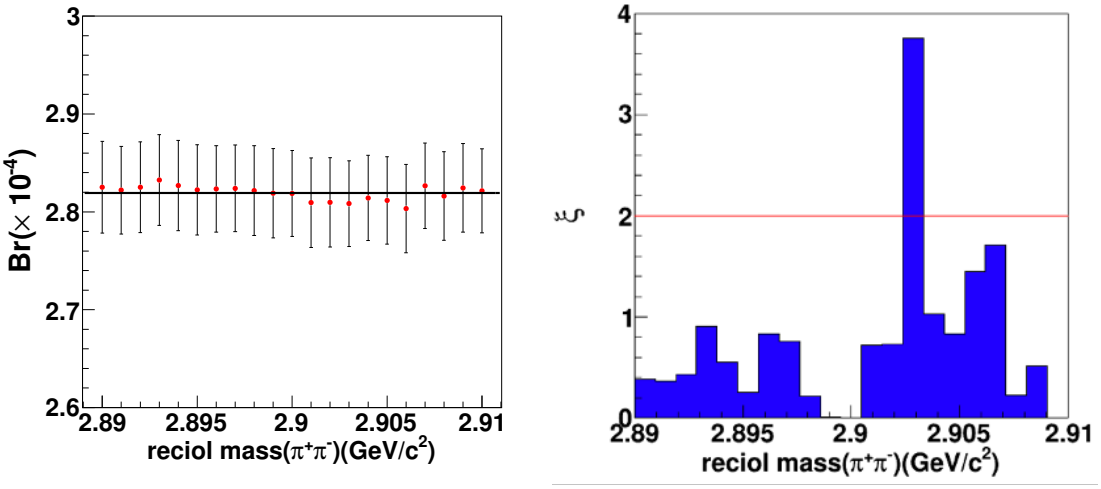

Fig. 15: The systematic uncertainties estimation using Barlow method

7.2.4 QED background estimation

To estimate the uncertainties of QED background events, changing QED background events in 1σ range, the differences are taken as the systematic uncertainties comparing the nominal values, 0.8% for $\psi(3686) \to \Sigma^-\bar{\Sigma}^+$.

7.2.5 Non-packground estimation

To estimate the uncertainties of background events, we changed the order of polynomial functions for background descriptions. The differences are taken as the systematic uncertainties comparing the nominal values, 0.8% for $\psi(3686) \to \Sigma^-\bar{\Sigma}^+$.

7.2.6 Peaking background

For the peaking background, we change the normalized numbers of fixed peaking background events in 1σ. The differences are taken as the systematic uncertainties comparing the nominal values, 0.4% for $\psi(3686) \to \Sigma^-\bar{\Sigma}^+$.

7.2.7 Kinematic fitting

With the track correction for the helix parameters, the χ^2_{1C} distribution should be more consistent between data and MC. Then we could use the difference between before correction and after correction as the systematic uncertainties, and take the value with correction as the nominal one. The differences are less than 0.2%, so this contribution is negligible.

7.2.8 Total number of $\psi(3686)$

The total number of $\psi(3686)$ mesons are based on inclusive hadronic events, as described in [25]. The uncertainties of the total number are determined to be 0.70% for $\psi(3686)$ events.

8 Summary

In summary, based on the 448.1×10^6 $\psi(3686)$ events collected at BESIII detector, the branching fractions and decay parameters of $\psi(3686) \to \Sigma^-\bar{\Sigma}^+$ are measured for the first time. The table summarizes the results of parameters of the angular distribution and branching fraction for this channel as Table 13.

Tab. 13: Summary of the angular distribution parameter and branching fraction of $\psi(3686) \to \Sigma^-\bar{\Sigma}^+$

Parameters	$\psi(3686) \to \Sigma^-\bar{\Sigma}^+$
$\alpha_{\psi(3686)}$	$0.96 \pm 0.09 \pm 0.03$
Branching fraction	$(2.83 \pm 0.04 \pm 0.08) \times 10^{-4}$

And by comparison the branching fractions of $J/\psi \to \Sigma^-\bar{\Sigma}^+$ and $\psi(3686) \to \Sigma^-\bar{\Sigma}^+$, the Q value of "12%" is tested to be $Q = \frac{P_{J/\psi}}{P_{\psi(3686)}} \times \frac{\psi(3686)\to\Sigma^-\bar{\Sigma}^+}{J/\psi\to\Sigma^-(n\pi^-)\bar{\Sigma}^+(\bar{n}\pi^+)} = \frac{1}{1.4194} \times \frac{2.83\pm0.08}{14.83\pm0.30} = 13.25\% \pm 1.05\%$ (The $\frac{P_{J/\psi}}{P_{\psi(3686)}}$ is correction factor of the phase space, where $P_{J/\psi}$ or $P_{\psi(3686)}$ is the Σ^- momentum in the J/ψ or $\psi(3686)$ decay process).

References

[1] S. J. Brodsky and G. P. Lepage, Phys. Rev. D 24, 2848 (1981).

[2] M. Claudson, S. L. Glashow and M. B. Wise, Phys. Rev. D 25, 1345 (1982).

[3] C. Carimalo, Int. J. Mod. Phys. A2, 249 (1987).

[4] T. Appelquist and H. Politzer, Phys. Rev. Lett. 34, 43 (1975).

[5] M. Ablikim et al. (BESIII Collaboration), Phys. Lett. B 614 37 (2005).

[6] Q. Wang, G. Li and Q. Zhao, Phys. Rev. D 85, 074015 (2012). M. E. B. Franklin et al. (MARKII Collaboration), Phys. Rev. Lett. 51, 963 (1983).

[7] P. A. Zyla *et al.* [Particle Data Group], PTEP **2021**, 083C01 (2021).

[8] M. Ablikim et al. [BESIII Collaboration], Phys. Rev. D 95, no. 5, 052003 (2017) doi:10.1103/PhysRevD.95.052003 [arXiv:1701.07191 [hep-ex]]

[9] M. Ablikim et al. [BESIII], [arXiv:2004.07701 [hep-ex]].

[10] https://hnbes3.ihep.ac.cn/HyperNews/get/AUX/2020/12/24(BAM-00476)

[11] M. Ablikim et al. (BESIII Collaboration), Nucl. Instrum. Meth. A 614, 345 (2010).

[12] C. H. Yu et al., Proceedings of IPAC2016, Busan, Korea, 2016, doi:10.18429/JACoW- IPAC2016-TUYA01.

[13] M. Ablikim et al. [BESIII Collaboration], Chin. Phys. C 44, 040001 (2020).

[14] X. Li et al., Radiat. Detect. Technol. Methods 1, 13 (2017); Y. X. Guo et al., Radiat. Detect. Technol. Methods 1, 15 (2017); P. Cao et al., Nucl. Instrum. Meth. A 953, 163053 (2020).

[15] G. Faldt (GF), Eur. Ph. J. A 52 141(2016); GF, A. Kupsc (AK), Phys. Lett. B 772 16(2017); GF, Phys. Rev. D 97 053002 (2018); GF, AK, S. Leupold, E. Perotti, arXiv:1809.04038 (2018).

[16] K. A. Olive et al. (Particle Data Group) Chin. Phys. C 38, 090001 (2014).

[17] S. Agostinelli et al. (geant4 Collaboration), Nucl. Instrum. Meth. A 506, 250 (2003).

[18] S. Jadach, B. F. L. Ward and Z. Was, Comp. Phys. Commu. 130, 260 (2000); Phys. Rev. D 63, 113009 (2001).

[19] D. J. Lange, Nucl. Instrum. Meth. A 462, 152 (2001); R. G. Ping, Chin. Phys. C 32, 599 (2008).

[20] J. C. Chen et al., Phys. Rev. D 62, 034003 (2000).

[21] https://docbes3.ihep.ac.cn/DocDB/0002/000250/026/Asymmetry%20Parameters%20Measurement.pdf

[22] M. Ablikim et al. (BESIII Collaboration), Phys. Rev. D **101**, no.9,092002(2020) doi:10.1103/PhysRevD.101.092002 [arXiv:2004.01394 [hep-ex]].

[23] https://indico.ihep.ac.cn/event/11850/contribution/0/material/slides/0.pdf

[24] https://hnbes3.ihep.ac.cn/HyperNews/get/paper504.html. BAM-00504: Study of tracking and PID systematic uncertainty, by Fang Liu et al.

[25] M. Ablikim et al. (BESIII Collaboration), Chin. Phys. C 37, 063001 (2013).

[26] Phys. Rev. D **79**, 052001 (2009).

[27] M. Ablikim et al. [BESIII], [arXiv:2004.07701 [hep-ex]].

[28] https://indico.ihep.ac.cn/event/13532/contribution/1/material/slides/0.pdf

Appendices

A ChangeLog

From Memo V4.7 to Memo V4.8.1:

The old and new results are shown in the Table 14, and the change of systematic uncertainties are shown in the Table 15, Table 16, Table 17, and Table 18.

Tab. 14: Change of results from CWR beginning to end.

Change	Br($\times 10^{-4}$)	Angular parameter α_B
Results of CWR beginning	$2.82 \pm 0.04 \pm 0.21$	$0.98 \pm 0.09 \pm 0.07$
Results of CWR end	$2.83 \pm 0.04 \pm 0.08$	$0.96 \pm 0.09 \pm 0.03$

The reason of nominal value change for branching fraction and angular parameter: In the updated version, we use the data collected at 3.65 GeV instead of 3.773 GeV datasets to estimate the non-$\psi(3686)$ backgrounds.

The reason of systematic uncertainty change from CWR beginning to end:

- MC efficiency correction: In previous version, we taken the maximum difference between data and MC as systematic uncertainty. However, based on suggestions from other reading group, the uncertainty is estimated by using this formula: $\delta = \sqrt{\sum_{i=1}^{n}(\frac{\epsilon_i-\epsilon_0}{\epsilon_0})^2}$, where n is the number of bins in different transverse momenta and polar angles, ϵ_0 is a nominal efficiency, and ϵ_i is a new efficiency when the scale factor is changed in 1σ for i bin.

- $M_{rec(\pi^+\pi^-)}$: Based on Sneha's suggestion, we remove this systematic uncertainty because the Barlow test is stable.

- Fitting range: For the systematic uncertainty from fit range, we remove it because this uncertainty has been included in the systematic uncertainty of background estimation.

- QED peaking background estimation: In the updated version, we use the data collected at 3.65 GeV instead of 3.773 GeV datasets to estimate the non-$\psi(3686)$ backgrounds. The statistics of 3.65 GeV are less than those of 3.773 GeV, so the systematic uncertainty becomes larger.

- Number of bins: It has also been updated again because nominal value has been changed.

- Fitting $\cos\theta$ range: It has also been updated again because nominal value has been changed.

398 • The systematic uncertainties of angular distribution parameter: Using the same method, the sys-
399 tematic uncertainties of angular distribution parameter have also been reconsidered because the
400 value of the nominal of each bin has changed.

Tab. 15: CWR beginning: Systematic uncertainties of the branching fraction measurement(%).

Source	Uncertainty (%)
MC efficiency correction	7.0
Decay parameter	1.2
$M_{rec(\pi^+\pi^-)}$	1.0
Fitting range	0.7
QED peaking background estimation	0.1
Non-peaking background estimation	0.8
Peaking background estimation	0.4
Kinematic fitting	0.2
Total number of $\psi(3686)$	0.7
Total	7.3

Tab. 16: CWR end: Systematic uncertainties of the branching fraction measurement(%).

Source	Uncertainty (%)
MC efficiency correction	1.9
Decay parameter	1.2
QED peaking background estimation	0.8
Non-peaking background estimation	0.8
Peaking background estimation	0.4
Kinematic fitting	0.2
Total number of $\psi(3686)$	0.7
Total	2.6

Tab. 17: CWR beginning: Systematic uncertainties of angular distribution measurement(%).

Source	Uncertainty(%)
MC efficiency correction	1.8
$M_{rec}(\pi^+\pi^-)$	3.7
Fitting range	1.8
QED peaking background estimation	negligible
Non-peaking background estimation	1.2
Peaking background estimation	1.4
Kinematic fitting	0.2
Number of bins	0.9
Fitting $\cos\theta$ range	1.9
Total	5.3

Tab. 18: CWR end: Systematic uncertainties of angular distribution measurement(%).

Source	Uncertainty(%)
MC efficiency correction	0.5
QED peaking background estimation	negligible
Non-peaking background estimation	1.2
Peaking background estimation	1.5
Kinematic fitting	0.3
Number of bins	0.4
Fitting $\cos\theta$ range	2.0
Total	2.9

Appendices

B $\bar{n}$ control sample

To study the $\bar{n}$ reconstruction efficiency, we choose the $J/\psi(\psi(3686)) \to p\bar{n}\pi^-$ as the control sample. The $\bar{n}$ transverse momentum distributed in the region from 0.5 to 1.4 GeV, which could cover our signal area.

Charged tracks reconstructed by main drift chamber(MDC) hit information must be fitted by Kalman method successfully and come from the interaction region in three dimensions. Due to changing beam conditions, the interaction point (IP) moves. Thus, a separate average IP is determined for each run using the VertexDbSvc package. Relative to this run-dependent IP, each charged track must satisfy the following requirements:

- $V_{xy} < 0.5$ cm,
- $|V_z| < 5$ cm,
- $|\cos\theta| < 0.93$,
- Good tracks is required $N = 2$.

Here, θ is the polar angle of the charged track with respect to the beam axis, V_{xy} and $|V_z|$ are the closest approaches of a charged track to the interaction point in the Oxy plane and in the z position.

B.1 Particle identification

The charged pions and p are identified via ParticleID package by using the TOF and dE/dx measurements with which the combined confidence levels $\mathscr{L}(\pi)$ and $\mathscr{L}(p)$ for pion and p hypotheses are calculated, respectively. The particle is considered to be π^- or p if the $Prob_{PID}$ more than any other particle hypothesis. We require the π^+ and π^- candidates satisfy the following criteria:

- $\pi^\pm$: $\mathscr{L}(\pi) > \mathscr{L}(p)$ and $\mathscr{L}(\pi) > \mathscr{L}(k)$,
- p or $\bar{p}$: $\mathscr{L}(p) > \mathscr{L}(\pi)$ and $\mathscr{L}(p) > \mathscr{L}(k)$,

B.2 $\bar{n}$ Shower Requirement

The cluster in the EMC which satisfies the following criteria is regarded as a good $\bar{n}$ shower:

- barrel EMC, $|\cos\theta| < 0.80$; endcap EMC, $0.86 < |\cos\theta| < 0.92$;

- At least one shower with energy larger than 0.6 GeV is required. Fig. 2 shows the deposit energy distribution of $\bar{n}$ and n in the EMC from MC simulation.

- Second moment> 20. The second momentum is defined as $\sum_i E_i r_i^2 / \sum_i E_i$, where E_i is the deposit energy in the i_{th} crystal and r_i is the radial distance of the crystal i from the cluster center.

- To suppress electronic noise and showers unrelated to the event, the difference between the EMC time and the event start time is required to be within (0, 700) ns

- The angle $\theta_{\bar{n},trk}$ between the $\bar{n}$ and the any charged track is larger than 10°.

B.3 $\bar{n}$ reconstruction efficiency

- fitting range: $M_{p\pi^- recoil} \in$ [0.85,1.05] GeV

- $\bar{n}$ reconstruction efficiency is defined as : $\frac{N_{\bar{n}}>=1}{N_{\bar{n}}>=0}$.

Appendices

C The momentum and anglular distributions between data and signal MC

The signal events are scaled by using our measuring branching ratio and background come from inclusive mc in the Fig. 16.

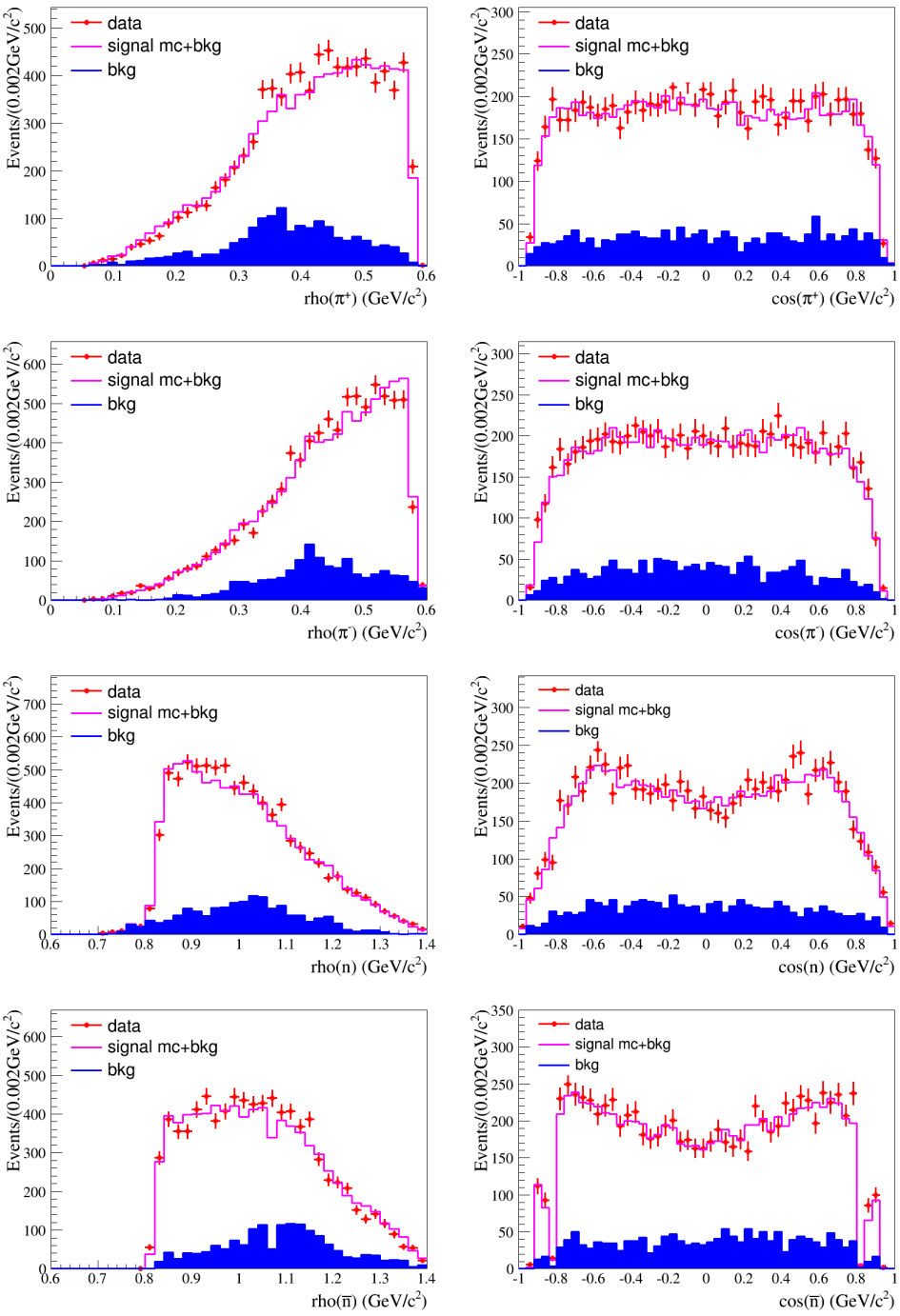

Fig. 16: The distributions of momentum and angle for final particle.

D Perform the I/O Check for the BF measurement

The samples are composed of signal mc and background which come from inclusive mc. The signal is described by the MC shape convoluted with Gaussian function which represents the difference between

data and MC in the resolution and mean value as the Fig 17. The output of branching ratio is consistence with input within one standard deviation(input: 2.79×10^{-4}, output: $(2.77 \pm 0.04) \times 10^{-4}$).

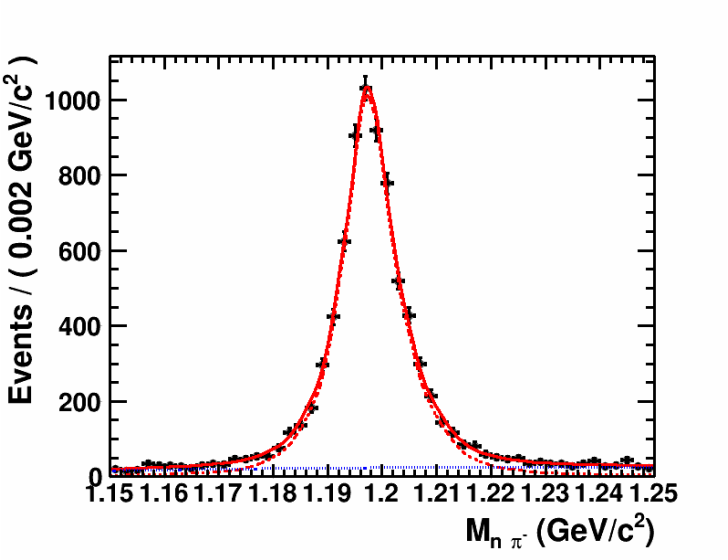

Fig. 17: The distributions of invariant mass for $n\pi^-$.

Appendices

E The measurement of branching ratio of $\psi(3686) \to \gamma\Sigma^+\bar{\Sigma}^-$

The branching fraction of peaking background channel $\psi(3686) \to \gamma\Sigma^-\bar{\Sigma}^+$ have been estimated by using decay channels of $\psi(3686) \to \gamma\Sigma^+\bar{\Sigma}^-$. The fitting results are shown in the Fig. 18.

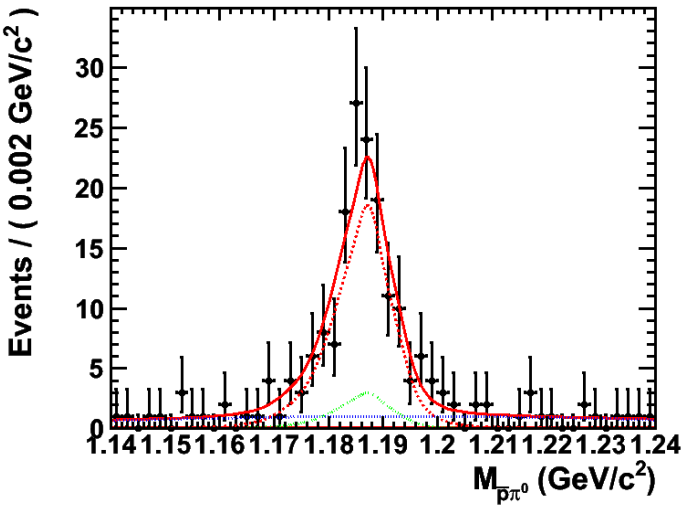

Fig. 18: The distributions of invariant mass for $\bar{p}\pi^0$.